

Actin Bundling: Initiation Mechanisms and Kinetics

Pavel Kraikivski, Boris M. Slepchenko, and Igor L. Novak

Richard D. Berlin Center for Cell Analysis and Modeling, Department of Cell Biology, University of Connecticut Health Center, Farmington, Connecticut 06030, USA

(Received 6 March 2008; published 17 September 2008)

Bundling of rapidly polymerizing actin filaments underlies the dynamics of filopodial protrusions that play an important role in cell migration and cell-cell interaction. Recently, the formation of actin bundles has been reconstituted *in vitro*, and two scenarios of bundle initiation, involving binding of two filament tips and, alternatively, linking of the tip of one filament to the side of the other, have been discussed. A first theoretical analysis is presented indicating that the two mechanisms can be distinguished experimentally. While both of them result counterintuitively in comparable numbers of bundles, these numbers scale differently with the average bundle length. We propose an experiment for determining which of the two mechanisms is involved in the *in vitro* bundle formation.

DOI: [10.1103/PhysRevLett.101.128102](https://doi.org/10.1103/PhysRevLett.101.128102)

PACS numbers: 87.16.Ka, 87.16.-b

Filamentous actin constitutes an important component of the cell cytoskeleton [1]. The structure and patterns of actin meshwork change dynamically as filaments polymerize, branch, and bundle, which enables living cells to vary their shape and migrate. One such dynamic pattern, used by cells to explore their environment and build adhesive outposts, are filopodia—long, fingerlike protrusions that result from the formation and growth of bundles of actin filaments [2–4]. The filaments are thought to be held in a bundle by linker proteins such as fascin [5]. Recently, actin bundles have been reconstituted *in vitro* in the presence, or after addition, of fascin [6,7]. In these experiments, the bundles emerge from a dense quasi-two-dimensional meshwork of actively polymerizing filaments and form starlike structures [Fig. 1(a)]. Importantly, the conditions of the *in vitro* polymerization and bundling are strongly nonequilibrium. This is due to the excess of fascin and Arp2/3, the protein promoting the nucleation of new filaments through branching [8]. In addition, the assays do not include any capping proteins or depolymerization factors.

It is generally accepted that the bundle arises from two filaments zipped up by a linker protein [6,7], but initiation mechanisms are a subject of active research. Two scenarios have been recently proposed [6,9,10]. One involves binding of two filament tips into a tip complex, which triggers the zipping if the filaments are at a sufficiently small angle [6,11–14]. In an alternate scenario, binding of the tip of one filament to the side of the other is thought to be sufficient for the initiation of linking [10], again on a condition of a small angle between the filaments. In this Letter, we analyze how the two mechanisms would affect the dynamics of bundling in order to determine if they are experimentally distinguishable. Our results indicate that while, surprisingly, both of them may result in comparable numbers of bundles, these numbers scale differently with the average linear size of the aster. Therefore, the mechanisms can be

distinguished by measuring the size dependence of the final number of bundles.

Development of the system of actin filaments and bundles in nonequilibrium assays is analyzed with the aid of a model, which accounts for four essential processes: Arp2/3-mediated nucleation of filaments, polymerization of filaments (both individual and in the bundle), initiation of a bundle from two unbundled filaments, and thickening of a bundle as it absorbs individual filaments [15] [Fig. 1(c)]. Effects of slower processes, such as depolymerization in the absence of depolymerization factors [7,16] and thermal fluctuations of the filaments [17], can be ignored because a pool of actin monomers in the *in vitro* assays is exhausted quickly due to the facilitated nucleation and rapid polymerization of filaments [7]. Aside from a small number of seed filaments, all new linear filaments nucleate from Arp2/3 complexes at the sides of the existing fila-

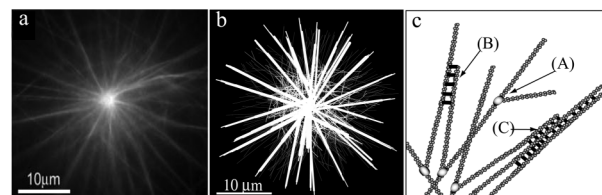


FIG. 1. (a) Starlike structure of actin bundles reconstituted *in vitro* (adapted from [7]). (b) Snapshot of the aster after depletion of monomers in a typical Monte Carlo realization based on Eq. (1). The parameters mimic experimental conditions in [7]: $Y_0 = 4.5 \times 10^6$, $(\tau_p)^{-1} = 75 \text{ s}^{-1}$, $(\tau_n)^{-1} = 5 \times 10^{-6} \text{ s}^{-1}$, and $\alpha_c \delta / h = 10^{-2}$ (the aster thickness h is on the order of several δ). Heavy lines are actin bundles; light lines depict free filaments. (c) Diagram of processes affecting dynamics of filaments and bundles: (A) nucleation of a linear filament, (B) initiation of a bundle (shown for the tip-side mechanism), and (C) incorporation of an unbundled filament into an existing bundle.

ments [Fig. 1(c), (A)] (new filaments do not nucleate from the bundles, possibly because of a dense decoration of those by the linker [5,6]). Because each nucleated filament has one point of origin and one growing tip, the whole branched system, despite its complexity, can be unambiguously described as a set of linear filaments. To initiate a bundle [Fig. 1(c), (B)] or to link an unbundled linear filament to an existing bundle [Fig. 1(c), (C)], the linker must bend the filaments. This is modeled as an “all-or-none” transition [11,13,14] depending on whether the angle between the filaments (or between a filament and a bundle) is below or above a critical value α_c , determined by cross-linking strength and elastic properties of the filaments and estimated to be in the range 0.005–0.5 [13,14].

Because of the abundance of the linker protein [7,18], the initiation of a bundle and the absorption of filaments by existing bundles are approximated as collision-controlled, so that the problem involves only two time scales determined by the initial frequency of polymerization events and the frequency of nucleation. The initial polymerization frequency is $\tau_p^{-1} = k_p C_0$, where k_p is the rate constant for binding of a monomer to a filament plus end and C_0 is the initial monomer concentration. For typical values of C_0 ($\sim 7.5 \mu\text{M}$) and k_p ($\sim 10 \mu\text{M}^{-1} \text{s}^{-1}$), $\tau_p^{-1} \approx 75 \text{s}^{-1}$ [7,19]. The Arp2/3-mediated nucleation involves two main steps: formation of a complex of Arp2/3 with one or two actin monomers and its subsequent attachment to an existing filament [20]. Consistently with the fact that the overall polymerization rate does not depend significantly on the mass of the seed filaments [21], we treat the complex formation as a time-limiting step, though the results are not affected by this assumption. The nucleation frequency depends on the Arp2/3 concentration. For saturating concentrations $\sim 0.1 \mu\text{M}$ used in the experiments, τ_n/τ_p is estimated to be on the order of 10^6 – 10^7 [19,22].

Formally, a state S of the system is defined by the number of monomers Y [23], the set of unbundled linear filaments $\{f_i: i = 1, \dots, X\}$, and the set of bundles $\{b_j: j = 1, \dots, B\}$: $S \equiv (Y, \{f\}, \{b\})$ (X and B are the numbers of free filaments and bundles, respectively) [25]. The linear filament is modeled as a two-dimensional vector with a fixed origin. The bundle b_j is defined by a backbone vector with a fixed origin and by a set of filaments f_{kj} , $k = 1, \dots, N b_j$, all of which have the direction of the backbone and are separated from it by the distance on the order of the monomer size δ ; the backbone length is defined as the maximum length of filaments in the bundle. The direction of a newly formed bundle is defined as a normalized sum of unit vectors of the filaments initiating the bundle to reflect their bending caused by the linker. The initial state of the system is $S_0 = (Y_0, \{f\}_0, \emptyset)$, where $\{f\}_0$ is a set of X_0 short, randomly oriented seed filaments of length L_0 with the “minus ends” placed randomly in $\Omega_0 \subset R^2$, $\sqrt{|\Omega_0|} \sim L_0$.

In our analysis, we utilize both detailed spatial simulations and mean-field approaches. The detailed dynamics

are described by the probability $P(S, t|S_0, 0)$ for the system to be in a state S at time t , given an initial state S_0 at $t = 0$. The governing equation [26]

$$\partial_t P = \sum_{S'(\neq S)} W_{S' \rightarrow S} P(S', t|S_0, 0) - W_{S \rightarrow S'} P(S, t|S_0, 0) \quad (1)$$

is solved numerically using kinetic Monte Carlo techniques [a snapshot of a typical realization is shown in Fig. 1(b)]. The transition rates $W_{S' \rightarrow S}$ in Eq. (1) are nonzero only for the intermediate states S' that are “separated” from S by a single transition corresponding to one of four processes included in the model [25]. Importantly, the transition rate for the bundle initiation involves a collision factor that depends on a particular mechanism: For the mechanism relying on the tip-tip binding, the factor is nonzero only when the distance between the two tips becomes sufficiently small (tip-tip collisions), whereas for the “tip-side” mechanism, this factor reflects a collision of the tip of one filament with the side of the other.

Insight into behavior of the system can also be gained from a nonspatial mean-field approximation formulated in terms of averages, such as $\langle B \rangle = \sum_S B(S) P(S, t|S_0, 0)$, etc., as it allows one to obtain important estimates based on analytical solutions [25]. In this approximation, the number of monomers Y , the total number of filaments E (both individual and in bundles), and the average linear size (radius) of the aster L form a closed system [25] yielding estimates for the characteristic time of aster formation, the final size of the aster (the aster size at $t \rightarrow \infty$), and the final number of all filaments:

$$\tau = \sqrt{2\tau_p \tau_n}, \quad L_\infty = \delta \sqrt{\frac{2\tau_n}{\tau_p}}, \quad E_\infty = Y_0 \sqrt{\frac{2\tau_p}{\tau_n}}. \quad (2)$$

(Here and below, the angular brackets denoting ensemble averaging are omitted for brevity.) The results (2), obtained in the limit $X_0/E_\infty \ll 1$, agree with the solutions of Eq. (1) [25]. Also, with the estimates of τ_p and τ_n as above, the characteristic time τ is in the 20- to 100-second range, which agrees with the experiments [7].

An upper bound for the number of bundles B can be obtained by ignoring incorporation of individual filaments into existing bundles. For the “tip-tip” mechanism, the upper mean-field estimate of the final number of bundles is [25]

$$B_\infty^{\text{tip-tip}} = \frac{8}{\pi^3} \frac{\alpha_c \delta}{h} Y_0^2 \left(\frac{\tau_p}{\tau_n}\right)^{3/2}, \quad (3)$$

where the aster thickness h is on the order of several δ . Indeed, $B_\infty^{\text{tip-tip}}$ can be viewed as the total number of “favorable” tip-tip collisions over the time τ : $B_\infty^{\text{tip-tip}} \approx \tau R_{\text{coll}}$, where the collision frequency R_{coll} is expressed in terms of the average relative velocity of the tips v_{rel} and the average tip density $\bar{\rho}_X$ as $R_{\text{coll}} = (\alpha_c/\pi) \delta^2 v_{\text{rel}} X \bar{\rho}_X$. Using

$v_{\text{rel}}\tau \sim L_{\infty}$, $\bar{\rho}_X \sim X/(L_{\infty}^2 h)$, and $X \sim E_{\infty}$, the final number of bundles is estimated as $B_{\infty}^{\text{tip-tip}} \sim (\alpha_c \delta^2/h) E_{\infty}^2/L_{\infty}$, which, with the account of Eqs. (2), is essentially equivalent to (3). Figure 2(a) illustrates agreement of the mean-field approximation (3) and the solution of Eq. (1) obtained for the tip-tip mechanism in the absence of filament absorption. Interestingly, the upper bound (3) provides a reasonably accurate approximation for the final number of bundles even when the filament absorption is taken into account, as illustrated by Fig. 2(b). In this case, the bundles become thicker, and the average number of filaments per bundle, shown in the inset in Fig. 2(b), is comparable with experimental observations in [27].

Intuitively, the tip-side mechanism should result in a much larger number of bundles because of a higher frequency of collisions. Indeed, the mean-field collision rate for this mechanism is $R_{\text{coll}} \propto X\bar{\rho}_M$, where $\bar{\rho}_M$ is the average density of the filamentous actin. However, spatial correlations in the system of filaments, not included in the mean-field approach, effectively reduce the number of favorable tip-side collisions. While the Monte Carlo simulations confirm that the frequency of all collisions is proportional to $X\bar{\rho}_M$, the local density of filamentous actin ρ_M , unlike ρ_X , is nonuniform in space and “out of phase” with the fraction of collisions occurring at a sufficiently small angle [Fig. 3(a)]. The latter is skewed towards the periphery of the system, indicating that elongated filaments have better chances to collide at a small angle. The resulting decrease in the number of favorable tip-side collisions leads to a counterintuitive conclusion: For realistic τ_p , τ_n , h , and α_c , both $B_{\infty}^{\text{tip-side}}$ and $B_{\infty}^{\text{tip-tip}}$ may fall into the experimentally observed range of tens to hundreds. Interestingly, the effect can be captured by simply reducing the mean-field estimate for the tip-side mechanism by a certain factor. As shown in Fig. 3(b), the corrected mean-

field result [25]

$$B_{\infty}^{\text{tip-side}} = \frac{\alpha_c^* \delta}{\pi^2 h} Y_0^2 \frac{\tau_p}{\tau_n}, \quad (4)$$

with $\alpha_c^* = 0.07\alpha_c$, accurately approximates the solution of Eq. (1) for the case of the tip-side binding.

Comparing Eqs. (3) and (4) with the account of (2) leads to an important observation: The final numbers of bundles in the two mechanisms scale differently with the final linear size of the aster: $B_{\infty}^{\text{tip-tip}} \propto (L_{\infty})^{-3}$ and $B_{\infty}^{\text{tip-side}} \propto (L_{\infty})^{-2}$. We therefore conclude that, while $B_{\infty}^{\text{tip-tip}}$ and $B_{\infty}^{\text{tip-side}}$ may fall in the same range due to possible variations in parameter values, their dependence on the final linear size of the aster is described by a power law with different exponents (Fig. 4), so the two mechanisms can be distinguished experimentally. For this, we propose to perform a series of the *in vitro* experiments, as described in Refs. [6,7], with a same initial concentration of actin monomers, and, after the polymerization is over, measure the number of bundles as a function of the linear size of the aster. The data are expected to be less noisy if the experiments are conducted with a fixed saturating concentration of fascin and with varying saturating amounts of Arp2/3. Our theory predicts that, in these conditions, the measured dependence will be described by the power law $B_{\infty} \propto (L_{\infty})^{-\beta}$. The data yielding $\beta \approx 3$ would indicate that the bundles initiate from the binding of the tips, whereas values of β between 1 and 2 would point to the tip-side mechanism. Our results also indicate (Fig. 2 in the supplementary material [25]) that, if both mechanisms function simultaneously, the tip-side mechanism dominates; i.e., virtually all bundles originate from the tip-side collisions, unless the tip-tip interaction is much stronger. In the latter

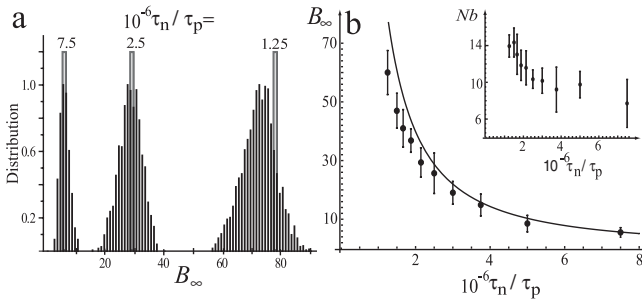


FIG. 2. The tip-tip mechanism: the number of bundles for varying τ_p and τ_n . (a) Mean-field estimates (3) vs numerical solution of Eq. (1) based on 10^2 to 10^3 realizations, for varying τ_n/τ_p . (b) Mean-field solution in the absence of filament absorption (solid line) and results of spatial simulations with absorption taken into account (dots with error bars); $\alpha_c \delta/h = 0.03$, $p = 5$; error bars correspond to a standard deviation based on 50–120 realizations. Inset: The average number of filaments per bundle Nb vs τ_n/τ_p .

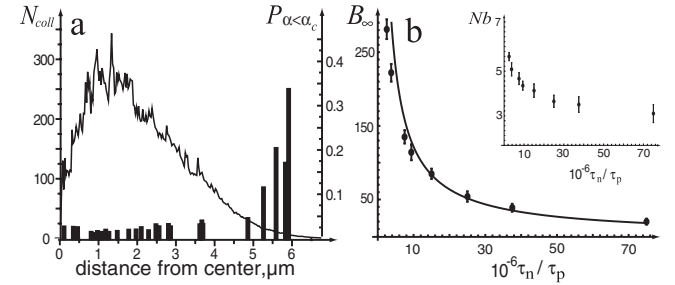


FIG. 3. The tip-side mechanism: numerical solution of Eq. (1) and mean-field estimates. (a) Number of all tip-side collisions N_{coll} (solid line) and fraction of collisions $P_{\alpha < \alpha_c}$ that occurred at a sufficiently small angle $\alpha < \alpha_c = 0.2$ (histogram), integrated over the first 30 s in one Monte Carlo realization and shown as functions of distance from the aster center. (b) Mean-field solution (4) in the absence of filament absorption (solid line) and results of spatial simulations with absorption taken into account (dots with error bars); $\alpha_c \delta/h = 0.03$, $p = 5$; error bars correspond to a standard deviation based on 50–120 realizations. Inset: The average number of filaments per bundle Nb vs τ_n/τ_p .

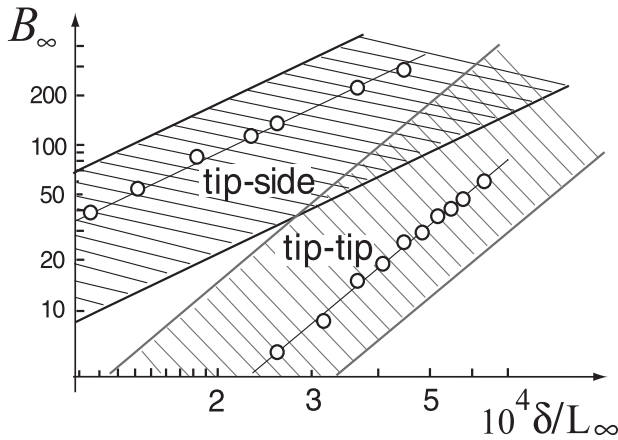


FIG. 4. $B_\infty - L_\infty$ diagram for the tip-tip and tip-side mechanisms in the log-log representation. Experimental data are expected to result in a band of points. While the width of the band depends on variations in $\alpha_c \delta/h$, reflecting varying abundance and activity of fascin, elasticity of filaments, thickness of the aster, etc., the slope of the band β , predicted to have different values for the two mechanisms of bundle initiation, can be used for distinguishing between them. Results of spatial stochastic simulations from Figs. 2(b) and 3(b) (open circles) are fitted by straight lines with the slopes $\beta \approx 1.6$ for the tip-side mechanism and $\beta \approx 2.8$ for the tip-tip mechanism. [The corresponding bands are shown for realistically possible ranges of $\alpha_c \delta/h$: (0.0005, 0.007) and (0.003, 0.05), for the tip-side and tip-tip initiation, respectively.]

case, the (B_∞, L_∞) data are fitted by the power law with β between 2 and 3.

In summary, we have analyzed the dynamics of bundling of actin filaments for two different mechanisms of bundle initiation. In one, binding of the tips of neighboring filaments initiates linking of the filaments into a bundle. In an alternative scenario, the initiation of a bundle is brought about by linking the tip of one filament to the side of the other. Our analysis indicates that, while both mechanisms may result in comparable numbers of bundles, the dependence of the final number of bundles on the final linear size of the aster is described by a power law with different exponents: $B_\infty \propto (L_\infty)^{-\beta}$, with $\beta \approx 3$ for the tip-tip mechanism and β between 1 and 2 for the tip-side mechanism; intermediate values of β would indicate presence of both mechanisms, with the tip-tip interaction being much “stickier” than that between the tip and the side. Based on these findings, we propose an experiment that would distinguish the two mechanisms in the *in vitro* conditions. The mathematical formalism developed here can be applied to modeling nonequilibrium dynamics of filopodia *in vivo*.

We acknowledge helpful conversations with Gary Borisy, Vladimir Rodionov, Leslie Loew, and Thomas Pollard. The work is supported by National Institutes of Health through Grants No. 1U54-RR022232, No. P41-RR13186, and No. 1U54-GM64346-01.

- [1] B. Alberts *et al.*, *Molecular Biology of the Cell* (Garland, New York, 1994), 3rd ed.
- [2] A. Jacinto and L. Wolpert, *Curr. Biol.* **11**, R634 (2001).
- [3] A. J. Ridley *et al.*, *Science* **302**, 1704 (2003).
- [4] P. Rorth, *Cell* **112**, 595 (2003).
- [5] T. M. Svitkina *et al.*, *J. Cell Biol.* **160**, 409 (2003).
- [6] D. Vignjevic *et al.*, *J. Cell Biol.* **160**, 951 (2003).
- [7] L. Haviv *et al.*, *Proc. Natl. Acad. Sci. U.S.A.* **103**, 4906 (2006).
- [8] T. D. Pollard, *Annu. Rev. Biophys. Biomol. Struct.* **36**, 451 (2007).
- [9] D. Vignjevic *et al.*, *Methods Enzymol.* **406**, 727 (2006).
- [10] S. F. Stewman and A. R. Dinner, *Phys. Rev. E* **76**, 016103 (2007).
- [11] J. Kierfeld, T. Kühne, and R. Lipowsky, *Phys. Rev. Lett.* **95**, 038102 (2005).
- [12] J. Kierfeld *et al.*, *J. Comput. Theor. Nanosci.* **3**, 898 (2006).
- [13] L. Yang *et al.*, *Biophys. J.* **90**, 4295 (2006).
- [14] X. Yu and A. E. Carlsson, *Biophys. J.* **87**, 3679 (2004).
- [15] Merging of bundles, another possible process, is ignored because these events are rare, with little effect on the overall dynamics.
- [16] T. D. Pollard *et al.*, *Annu. Rev. Biophys. Biomol. Struct.* **29**, 545 (2000).
- [17] J. R. Kuhn and T. D. Pollard, *Biophys. J.* **88**, 1387 (2005).
- [18] Y. Yamakita *et al.*, *J. Biol. Chem.* **271**, 12 632 (1996).
- [19] T. D. Pollard, *J. Cell Biol.* **103**, 2747 (1986).
- [20] R. D. Mullins *et al.*, *Proc. Natl. Acad. Sci. U.S.A.* **95**, 6181 (1998).
- [21] D. Pantaloni *et al.*, *Nat. Cell Biol.* **2**, 385 (2000).
- [22] M. A. Mogilner and L. Edelstein-Keshet, *Biophys. J.* **83**, 1237 (2002).
- [23] Diffusion of monomers is fast on a spatial scale of the aster [24].
- [24] V. C. Abraham *et al.*, *Biophys. J.* **77**, 1721 (1999).
- [25] See EPAPS Document No. E-PRLTAO-101-024839 for an appendix containing a detailed description of our model. For more information on EPAPS, see <http://www.aip.org/pubservs/epaps.html>.
- [26] C. W. Gardiner, *Handbook of Stochastic Methods for Physics, Chemistry and the Natural Sciences* (Springer-Verlag, Berlin, 2004).
- [27] Y. Tseng *et al.*, *J. Mol. Biol.* **310**, 351 (2001).